

# Effects of halo substructure on the power spectrum and bispectrum

Derek Dolney,<sup>\*</sup> Bhuvnesh Jain,<sup>\*</sup> Masahiro Takada<sup>\*</sup>

*Department of Physics and Astronomy, University of Pennsylvania, 209 S 33RD ST FL 2, Philadelphia, PA 19104-6396, USA*

Accepted 2004 May 5. Received 2004 April 6; in original form 2004 January 9

## ABSTRACT

We study the effects of halo substructure and a distribution in the concentration parameter of haloes on large-scale structure statistics. The effects on the power spectrum and bispectrum are studied on the smallest scales accessible from future surveys. We compare halo-model predictions with results based on  $N$ -body simulations, but also extend our predictions to 10-kpc scales which will be probed by future simulations. We find that weak-lensing surveys proposed for the coming decade can probe the power spectrum on small enough scales to detect substructure in massive haloes. We discuss the prospects of constraining the mass fraction in substructure in view of partial degeneracies with parameters such as the tilt and running of the primordial power spectrum.

**Key words:** galaxies: haloes – cosmological parameters – dark matter.

## 1 INTRODUCTION

The substructure of dark-matter haloes is a topic of interest in cosmology, especially due to its relevance to the cold-dark-matter model, which requires some degree of clumpiness to the matter distribution. In a recent paper, Kochanek & Dalal (2003) argue that substructure provides the best explanation (originally proposed by Mao & Schneider 1998) of the anomalous flux ratios found in gravitational lens systems. However, the observed number of dwarf galaxy satellites in the Local Group is more than an order of magnitude smaller than the number of subhaloes found in numerical simulations (Klypin et al. 1999; Moore et al. 1999a).

Observable statistics of the matter distribution provide an approach to substructure studies that is complementary to studies of strong-lens systems or direct observations of satellite galaxies. Substructure effects are expected to produce an observable effect in the power spectrum in the next generation of lensing surveys. As we show in this paper, substructure effects in the weak-lensing regime probe cluster scales primarily, as opposed to strong-lensing systems, which probe galactic scales.

The halo model provides a description of non-linear gravitational clustering which allows statistical quantities of interest to be efficiently computed. The essential concepts of the halo model were used by Neyman & Scott (1952) to describe the spatial distribution of galaxies over fifty years ago. Their results were later generalized by Scherrer & Bertschinger (1991). By combining the formalism of Scherrer & Bertschinger with results from  $N$ -body simulations such as a halo density profile (e.g. that of Navarro, Frenk & White 1997) and a halo mass function and bias parameters (e.g. Sheth & Tormen 1999), one is able to calculate various dark-matter and galaxy clustering statistics (Ma & Fry 2000; Seljak 2000; Peacock

& Smith 2000; Scoccimarro et al. 2001; Cooray & Hu 2001). See Cooray & Sheth (2002) for a comprehensive review of the halo model.

Most work on the halo model approximates haloes as spherically symmetric objects, described by a mass density which is a smoothly-decreasing function only of the distance from the halo centre. However, the density distribution of haloes which form in  $N$ -body simulations is not at all smooth (Navarro et al. 1997; Moore et al. 1999b). Rather, one finds that about 10 per cent of the mass is associated with subhaloes (Tormen, Diaferio & Syer 1998; Ghigna et al. 2000). In the large-scale structure literature to date, the effects of halo substructure are typically assumed to be small for purposes of calculating statistics of the dark-matter distribution. This paper explores the validity of this assumption. We will make quantitative statements about the size of substructure effects on the 2D and 3D dark-matter power spectra and bispectra. We will identify the length and angular scales at which halo substructure becomes important.

The results of  $N$ -body simulations also suggest a distribution of halo concentration parameters (Bullock et al. 2001; Jing 2000). Like substructure, this effect is often ignored, though the formalism to include it in the halo model is straightforward (Cooray & Hu 2001). This paper will quantify the effect of a concentration parameter distribution on the power spectra.

## 2 THEORY

To model substructure in a halo, the total mass  $M$  of the halo is divided into a smoothly distributed component of mass  $M_s$ , and the remaining mass  $m$  is placed in subhaloes. We will use the terms subhalo and subclump interchangeably. Ignoring substructure, the halo model requires specification of the halo density profile and the mass function, i.e. the number density of haloes of a given mass.

<sup>\*</sup> E-mail: dolney@astro.upenn.edu (DD); bjain@physics.upenn.edu (BJ); mtakada@hep.upenn.edu (MT)

To include substructure, one must specify not only the density profile of the smooth component, the Fourier transform of which we denote  $M_s U(k; M_s)$ , but also the density profile of the subhaloes, with Fourier transform  $m u(k; m)$ . The mass factors simply provide the proper normalization;  $U(k; M_s)$  and  $u(k; m)$  are normalized to unity. Suitable mass functions for the number density both of parent haloes,  $dN/dM$ , and of subhaloes,  $dn/dm$ , are also needed. In addition, the distribution of subhaloes within the parent halo must be specified. We denote its Fourier transform by  $U_c(k; M_s)$ . Using these ingredients, Sheth & Jain (2003) derive expressions for the power spectrum and the bispectrum. We give some results from their paper that are relevant to this work in the Appendix.

We use the mass function of Sheth & Tormen (1999) for the number density of parent haloes of a given mass  $M$ :

$$dM \frac{dN(M)}{dM} = \frac{\bar{\rho}}{M} A [1 + (a\nu)^{-p}] \sqrt{a\nu} e^{-a\nu/2} \frac{d\nu}{\nu}, \quad (1)$$

where  $\bar{\rho}$  denotes the average density of the Universe at the present epoch, and

$$\nu(M, z) := \left[ \frac{\delta_c(z)}{D(z)\sigma(M)} \right]^2 \quad (2)$$

is the peak height defined in terms of  $\delta_c(z)$ , the threshold over-density in the spherical-collapse model,  $D(z)$ , the growth factor for density perturbations, and  $\sigma(M)$ , the rms fluctuations in the matter density field at the present epoch smoothed with a top-hat window of radius  $(3M/4\pi\bar{\rho})^{1/3}$ . The normalization constant is fixed by requiring that all mass be contained within a parent halo, and turns out to be  $A = 0.116$ . For  $\delta_c$ , we use the fitting formula of Henry (2000). We use haloes with mean interior density 180 times the background density and take  $a = 0.67$  and  $p = 0.33$ , so that our mass function is universal (White 2002). The notation of this paper reflects our choice of halo boundary:  $r := r_{180b}$ ,  $M := M_{180b}$  and  $c := r_{180b}/r_s$ , where  $r_s$  is the usual scale radius parameter of the halo density profile.

We use the density profile of Navarro et al. (1997), hereafter NFW, for both the smooth component and the subhaloes. Its Fourier transform is most efficient to compute using sine and cosine integrals:

$$U(k, m) = \cos \kappa \{ \text{Ci}[\kappa(1+c)] - \text{Ci}(\kappa) \} - \frac{\sin \kappa c}{\kappa(1+c)}, \quad (3)$$

with  $\kappa := kr_{180b}/c$ ,

$$\text{Si}(x) := \int_0^x dr \frac{\sin r}{r} \quad (4)$$

and

$$\text{Ci}(x) := - \int_x^\infty dr \frac{\cos r}{r}. \quad (5)$$

We assume the distribution of subhaloes within a parent halo follows the mass distribution of the smooth component. That is,  $U_c(k; M_s)$  is also given by the NFW profile, normalized to unity. Simulations suggest that the abundance of subhaloes in the parent halo traces the density profile of the parent quite well except in the most dense region near its centre where the abundance of subhaloes is lessened due to tidal disruptions. The subhalo abundance in the inner region is not yet well resolved in simulations. Chen, Kravtsov & Keeton (2003) propose a modified NFW profile that is constant or zero inside of a core radius which they take to be 10–20 kpc for a  $10^{12} M_\odot$  halo. For a halo of this mass, only 4 per cent of its matter lies within the core radius. Hence, we use the latter profile,

the effect would be to move only 4 per cent of our subhaloes further from the centre. We will comment briefly on the effect we expect this to have on the power spectrum in the Discussion.

We use the concentration parameters found by Bullock et al. (2001), for all three profiles at redshift  $z$ , which are

$$\bar{c}(M, z) = 9(1+z)^{-1} \left[ \frac{M_{\text{vir}}(M)}{M_*} \right]^{-0.13} \quad (\text{smooth}), \quad (6)$$

for the smooth component of a halo and

$$\bar{c}(m, z) = 7.5(1+z)^{-1} \left[ \frac{m_{\text{vir}}(m)}{M_*} \right]^{-0.30} \quad (\text{subhalo}), \quad (7)$$

for all subhaloes. The non-linear mass scale  $M_*$  is defined by the relation  $\nu(M_*, 0) = 1$ . The translation  $M_{\text{vir}}(M)$  between different halo mass definitions is derived in the appendix of Hu & Kravtsov (2003). Bullock et al. find that the concentration parameter for subhaloes has some dependence on the local density around the subhalo. We ignore this effect here, as it is difficult to include in our model, and we do not believe inclusion would seriously affect our conclusions. Huffenberger & Seljak (2003) find a different concentration parameter by  $\chi^2$  minimization against the non-linear fitting formula of Smith et al. (2003):

$$\bar{c}(M, z) = 11(1+z)^{-1} \left( \frac{M}{M_*} \right)^{-0.05}. \quad (8)$$

Numerical simulations suggest a log-normal distribution for the concentration parameter about the mean value  $\bar{c}$ ,

$$p(c; m, z) dc = \frac{d(\ln c)}{\sqrt{2\pi\sigma_{\ln c}^2}} \exp \left\{ -\frac{\ln^2[c/\bar{c}(m, z)]}{2\sigma_{\ln c}^2} \right\}, \quad (9)$$

with a width  $\sigma_{\ln c} = 0.3$  (Jing 2000; Bullock et al. 2001). Unless otherwise noted, we use the mean values given in equations (6) and (7).

We assume a biasing prescription for the clustering of parent haloes. That is, the halo power spectrum is given in terms of the linear mass power spectrum  $P_L(k)$  as

$$P(k, z; M_1, M_2) = b_1(\nu_1) b_1(\nu_2) P_L(k, z), \quad (10)$$

where  $\nu_i := \nu(M_i, z)$ . We use the bias parameter of Sheth & Tormen (1999):

$$b_1(\nu) = 1 + \frac{a\nu - 1}{\delta_c} + \frac{2p/\delta_c}{1 + (a\nu)^p}. \quad (11)$$

For the subhaloes, we assume a power-law mass function suggested by numerical simulations (Tormen et al. 1998; Ghigna et al. 2000):

$$\frac{dn(m; M)}{dm} dm = N_0 \left( \frac{M}{m} \right)^\mu \frac{dm}{m}, \quad (12)$$

where  $\mu < 1$ . The normalization  $N_0$  is determined by the mass fraction contained in subhaloes,  $f$ :

$$f := \frac{M - M_s}{M} = \int dm \frac{m}{M} \frac{dn(m; M)}{dm}. \quad (13)$$

Numerical simulations suggest  $\mu \approx 0.9$  and  $f \approx 10$  per cent. We use these values unless otherwise noted. In addition, simulations suggest that subhaloes heavier than 1 per cent of the total mass in the parent halo are rare (Tormen et al. 1998; Chen et al. 2003), so we only include subhaloes with masses  $m \leq 0.01M$ .

We calculate the weak-lensing convergence using Limber's

approximation (Limber 1953; Kaiser 1992), so that the convergence power spectrum and bispectrum are given by

$$P^\kappa(l) = \int_0^{\chi_s} d\chi \frac{W^2(\chi)}{d_A^2(\chi)} P\left(\frac{l}{d_A(\chi)}\right) \quad (14)$$

and

$$B^\kappa(l_1, l_2, l_3) = \int_0^{\chi_s} d\chi \frac{W^3(\chi)}{d_A^4(\chi)} B\left(\frac{l_1}{d_A(\chi)}, \frac{l_2}{d_A(\chi)}, \frac{l_3}{d_A(\chi)}\right). \quad (15)$$

In the next section we will also use the reduced bispectrum, defined as  $B/3P^2$  for equilateral triangles.

We use the standard weak-lensing weight function (see, e.g. Bartelmann & Schneider 2001)

$$W(\chi) = \frac{3}{2} \Omega_m H_0^2 a^{-1} \frac{d_A(\chi) d_A(\chi_s - \chi)}{d_A(\chi_s)}, \quad (16)$$

where  $\chi$  is the comoving distance,  $\chi_s$  is the comoving distance of the source galaxies,  $d_A(\chi)$  is the comoving angular diameter distance and  $H_0$  is the present-day value of the Hubble parameter. For simplicity, we place all source galaxies at redshift 1.

We will calculate the covariance of the convergence field by adopting a binning scheme. Let  $P_i^\kappa$  denote the power averaged over a bin of width  $\Delta_i$  centred on the mode  $l_i$ . Our bins are chosen to have width  $\Delta_i/l_i = 0.3$ . In this notation, the covariance can be expressed as (Cooray & Sheth 2002; Meiksin & White 1999)

$$C_{ij} = \frac{1}{4\pi f_{\text{sky}}} \left\{ \frac{4\pi}{l_i \Delta_i} \left[ P_i^\kappa + \frac{\sigma_{\gamma_x}^2}{\bar{n}} \right]^2 \delta_{ij} + T^\kappa(l_i, -l_i, l_j, -l_j) \right\}, \quad (17)$$

where  $f_{\text{sky}}$  is the fraction of the sky surveyed,  $\sigma_{\gamma_x}$  is the per component rms intrinsic ellipticity of the sample galaxies,  $\bar{n}$  is the average galaxy number density in the survey. The first term is the sample variance; the second the shot noise. The last term,  $T^\kappa$ , is the trispectrum contribution, arising from non-Gaussianity in the convergence field.

It is likely that a space-based deep imaging survey will offer the best prospects for probing the small scales where substructure effects are important. We adopt parameters expected for the *SNAP* satellite lensing survey (e.g. Massey et al. 2003):  $\bar{n} = 100 \text{ gal/arcmin}^2$ ,  $f_{\text{sky}} = 2$  per cent,  $\sigma_{\gamma_x} = 0.34/\sqrt{2} = 0.24$ .

We use the covariance of the power spectrum to perform a least-squares fitting to a fiducial model  $\bar{P}^\kappa$  by calculating  $\chi^2$ ,

$$\chi^2 = \sum_{ij} (P_i^\kappa - \bar{P}_i^\kappa) C_{ij}^{-1} (P_j^\kappa - \bar{P}_j^\kappa), \quad (18)$$

and identifying  $1\sigma$ ,  $2\sigma$  and  $3\sigma$  contours as those with  $\Delta\chi^2 = 2.30$ , 6.17 and 11.8, respectively, which is appropriate for the two-parameter fits we will use.

We use a  $\Lambda$ CDM cosmological model with parameters  $\Omega_m = 0.3$ ,  $\Omega_\Lambda = 0.7$ ,  $\Omega_b = 0.05$ ,  $h = 0.7$ ,  $\sigma_8 = 0.9$  and the BBKS transfer function (Bardeen et al. 1986) with the shape parameter of Sugiyama (1995).

### 3 RESULTS

Fig. 1 compares halo-model calculations of the three-dimensional power spectrum with the non-linear fitting formula of Smith et al. (2003). In this figure, different fractions of the halo mass are placed in substructure. Adding substructure can be seen to increase power

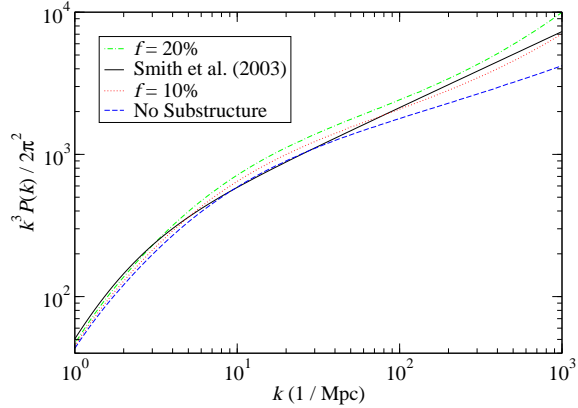


**Figure 1.** Halo-model calculations of the dimensionless power spectrum with different fractions of the halo mass placed in NFW subhaloes.

at scales  $k \gtrsim 1 \text{ Mpc}^{-1}$ . Substructure models predict more power than Smith et al. for  $10 \lesssim k \lesssim 100 \text{ Mpc}^{-1}$ , but the model with 10 per cent of the halo mass in substructure shows better agreement at smaller scales (though it should be noted that Smith et al. has been extrapolated beyond  $k \gtrsim 40 h \text{ Mpc}^{-1}$ ). The power spectrum is fairly insensitive to the exponent of the subhalo mass function,  $\mu$ . Reducing  $\mu$  from 0.9 to 0.7 can increase the power spectrum by about 4 per cent at length scales  $k \gtrsim 1 \text{ Mpc}^{-1}$ .

In Fig. 2 we divide the power spectrum into contributions from the various terms in equations (A3)–(A7). On scales  $k < 200 \text{ Mpc}^{-1}$ , the substructure contribution to the power spectrum is dominated by the density correlation between the smooth component of the parent halo and a subclump, denoted  $P_{\text{sc}}$ . The correlation of the density in a single subclump,  $P_{1c}$ , or between two different subclumps,  $P_{2c}$ , is negligible for parameter values of interest except for very high wavenumbers (where baryonic effects are likely to play a role). One should also note that the power of the smooth component only,  $P_{\text{ss}}$ , still dominates all other contributions on all scales considered, except for the largest scales where the two-halo term,  $P_{2h}$ , models the linear power spectrum.

In Fig. 3, we leave the integral over subhalo mass uncalculated for the  $P_{1c}$  and  $P_{\text{sc}}$  terms, so that one can see which subhalo masses provide the most power. The figures suggest that most of the extra power due to substructure between  $10 \lesssim k \lesssim 100 \text{ Mpc}^{-1}$ , comes from subhaloes of mass  $10^{10} \lesssim m \lesssim 10^{12} M_\odot$ . Subhaloes of this mass are likely contained in parent haloes of mass  $\gtrsim 10^{12} \text{--} 10^{14} M_\odot$ . Finally, since the weak-lensing efficiency peaks for  $z \approx 0.3\text{--}0.5$ , the conclusion is that the weak-lensing power spectrum can probe intermediate-redshift group and cluster mass haloes (provided the signal-to-noise permits its measurement as discussed below). This should make weak lensing as a probe of substructure a good complement to studies of strong lensing of quasars, which probe substructure in galactic haloes.

In Fig. 4 we plot a number of power spectra calculated with various models. Henceforth, curves titled ‘Bullock et al. (2001)’ and ‘Huffenberger & Seljak (2003)’ refer to halo-model calculations without substructure, using the concentration parameters found in those references. It should be noted that Huffenberger & Seljak obtained their concentration parameter by fitting to Smith et al. (2003) only up  $k = 40 h \text{ Mpc}^{-1}$ . Both Huffenberger & Seljak and Smith et al. have been extrapolated beyond  $k = 40 h \text{ Mpc}^{-1}$ ,

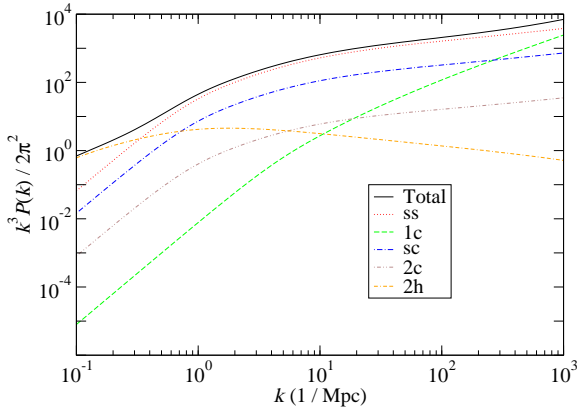


**Figure 2.** The dimensionless power spectrum separated into the contributions from each of the terms in equations (A3)–(A7). The order of the lines in the legend matches the order at  $k = 10^3 \text{ Mpc}^{-1}$ .

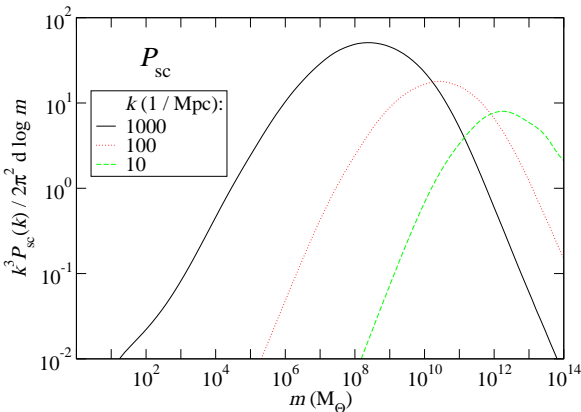


**Figure 3.** Contributions from the smooth-subclump term to the power spectrum per logarithmic mass bin. Integrating these curves against  $d \log m$  gives  $P_{sc}(k)$ .

and the apparently poor agreement of their model with Smith et al. beyond this wavelength should be attributed to this extrapolation.

It is apparent that adding either substructure or the concentration parameter distribution affects power only on scales  $k \gtrsim 10 \text{ Mpc}^{-1}$ . Substructure provides a 10–60 per cent increase in power on the scales  $10 \leq k \leq 1000 \text{ Mpc}^{-1}$ , with the largest factor corresponding to the smallest scales. The  $c$ -distribution provides only a 6–10 per cent increase in power over the same scales.

It is interesting to note that while the substructure model increases power relative to Smith et al. (2003) or Bullock et al. (2001), the concentration parameter of Huffenberger & Seljak (2003) decreases the relative power. And so, while all models may be consistent with Smith et al. at scales  $k \leq 10 \text{ Mpc}^{-1}$ , the better model should reveal itself as smaller scales are probed in higher-resolution simulations and observations. If the halo model is an appropriate physical description of mass clustering, then the sub-

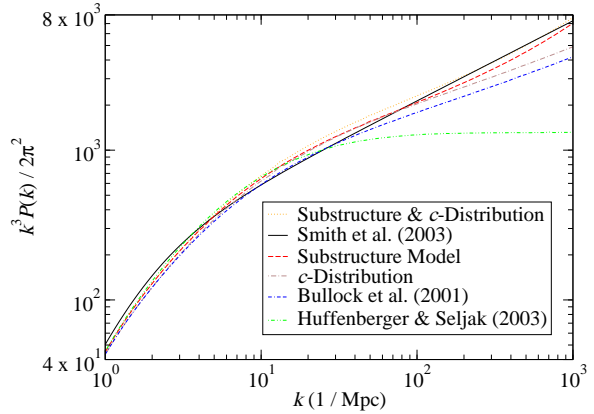


**Figure 4.** Comparison of dark-matter power spectra predicted by various models, including substructure, a log-normal distribution of halo concentration parameters as in equation (9), and the non-linear fitting formula of Smith et al. The order of the lines in the legend matches the order at  $k = 10^3 \text{ Mpc}^{-1}$ .

structure model presented here should provide the most robust predictions for the power spectrum on small scales.

In Fig. 5 we show the dimensionless convergence power spectrum predictions for the various models, assuming source galaxies at redshift 1. Again,  $c$ -distribution and substructure each provide about a 10 per cent increase in power at small scales, though the effect of substructure gets larger for the smallest scales. The halo-model calculations are discrepant with Smith et al. (2003) at the 10–20 per cent level. Most of the contribution to  $P^k(l)$  for  $10^3 \leq l \leq 10^5$  comes from  $P(k)$  with  $1 \leq k \leq 100 \text{ Mpc}^{-1}$ . At these scales, the transition between the one-halo and two-halo terms is important. Zehavi et al. (2003) have proposed a scale-dependent correction to the bias parameter and a method to account for halo exclusion that may improve the halo model on intermediate scales. Takada & Jain (2003) employ an approximate correction for halo exclusion to obtain a more well-behaved three-point correlation function on scales  $\approx 1 \text{ Mpc}$ . Given the error bars expected from future surveys, it is clear that improved precision in simulations as well as model predictions is needed. Some additional cosmological models are plotted in Fig. 6, which we will comment more on shortly.

In Figs. 7 and 8, we plot the predicted three-dimensional bispectrum and convergence bispectrum. It is interesting to note that, though substructure increases the bispectra, it causes a decrease in the reduced bispectra. That is, the substructure contribution to the power spectrum factor in the denominator exceeds its contribution to the numerator in the reduced bispectrum. This is due to the fact that the dominant substructure terms are the smooth-subclump for the power spectrum and the smooth-smooth-subclump term for the bispectrum. The  $P_{sc}$  term scales as  $(1 - f)f$ , while the  $B_{ssc}$  term scales as  $(1 - f)^2f$ , so the reduced bispectrum scales as  $1/f$  over most scales. Thus by using both the bispectrum and power spectrum, degeneracies between the substructure fraction and other cosmological parameters can be broken. We discuss this further in Section 4.

Shown in Fig. 9 is the substructure contribution to the bispectrum separated into each of the terms in equations (A10)–(A15). On the scales of interest, the substructure contributions to the bispec-

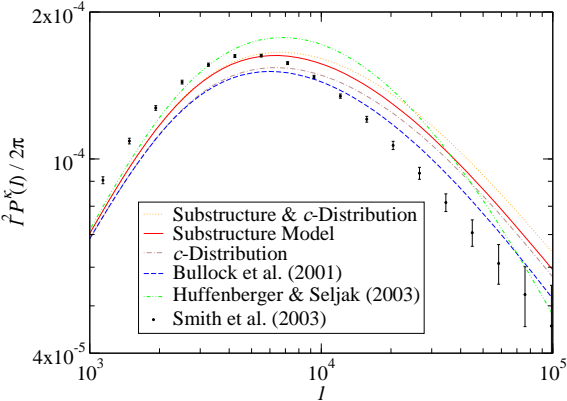


**Figure 5.** Various model predictions of dimensionless convergence power spectrum. Compares the substructure model and  $c$ -distribution to non-substructure models. The error bars are the diagonal part of the covariance calculated with equation (17) assuming  $\bar{n} = 100$  gal/arcmin $^2$ ,  $f_{\text{sky}} = 2$  per cent and  $\langle \gamma_{\text{int}}^2 \rangle^{1/2} = 0.34$ . The trispectrum contribution to equation (17) is approximated by a halo-model calculation. The order of the lines in the legend matches the order at  $l = 10^5$ .

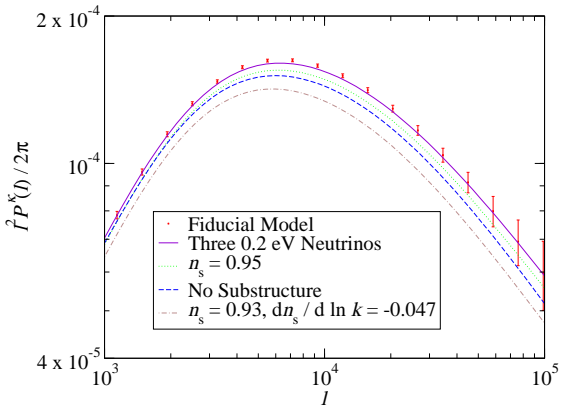


**Figure 6.** Dimensionless convergence power spectra for models with other phenomena that produce effects similar to substructure. The error bars are the diagonal part of the covariance calculated with equation (17) as in Fig. 5. The order of the lines in the legend matches the order at  $l = 10^5$ .

trum are dominated by the smooth-smooth-subclump term,  $B_{\text{ssc}}$ , and the bispectrum for individual subclumps,  $B_{1c}$ . The meaning of these terms is discussed more completely in the Appendix. It is interesting that the bispectrum contribution from single subhaloes,  $B_{1c}$ , provides a larger contribution than the smooth component alone,  $B_{\text{sss}}$ , for  $k \approx 10^3$  Mpc $^{-1}$ , but on these scales a purely gravitational calculation is not likely to be valid.

Results from the *WMAP* satellite have constrained the tilt and run of the primordial power spectrum. Tilt affects the small scale power in a way similar to substructure (cf. Fig. 6), so we consider next the feasibility of weak lensing to separate the effects of substructure from tilt and run in the primordial power spectrum. The results of examining the three parameter  $\chi^2(f, n_s, dn_s/d \ln k)$  are shown in Fig. 10. We use the  $f = 10$  per cent substructure model

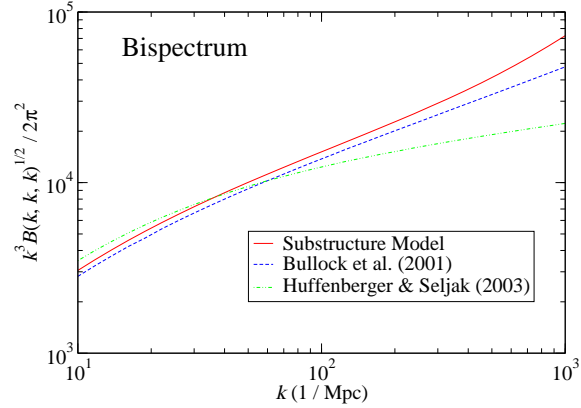


**Figure 7.** Various model predictions of the equilateral bispectrum. The upper panel shows the dimensionless equilateral bispectrum; the lower panel is the equilateral reduced bispectrum.

as the fiducial model, and calculate the  $\chi^2$  for  $P^k(l)$  relative to the fiducial model using modes in the range  $10^3 \leq l \leq 10^5$ . The covariance matrix used is that in equation (17). In the upper panel, we assume no running and use  $n_s = 1.00$  for the fiducial model. In the lower panel, we fix  $n_s = 0.93$  and allow a running spectral index, as described in Spergel et al. (2003), to vary about a fiducial value of  $dn_s/d \ln k = -0.047$  (Spergel et al. 2003). Note that we do not marginalize over the third parameter in these figures. We also apply priors as expected from the upcoming *Planck* mission:  $\sigma_{n_s} = 0.008$  and  $\sigma_{dn_s/d \ln k} = 0.004$  (Eisenstein, Hu & Tegmark 1998). These figures suggest that with cosmic microwave background (CMB) priors, future surveys that can measure  $P^k$  down to 0.1-arcmin scales can constrain the substructure mass fraction to about  $\pm 2$  per cent.

#### 4 DISCUSSION

We have shown that on small scales, the contribution of CDM substructure is important in accurate predictions of the power spectrum. In particular, it may help resolve the small scale discrepancy between  $N$ -body simulation results and the halo model. Our model with 10 per cent substructure and a concentration parameter distribution fits the small scale power spectrum extrapolated from Smith

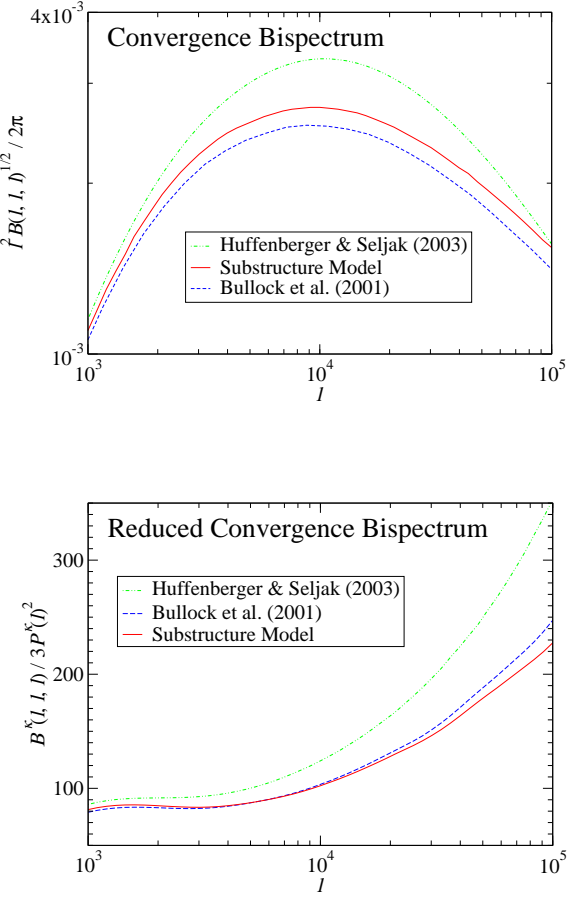


**Figure 8.** Various model predictions of the equilateral convergence bispectrum. Only the one-halo term is plotted. The upper panel shows the dimensionless equilateral convergence bispectrum; the lower panel is the equilateral reduced convergence bispectrum.

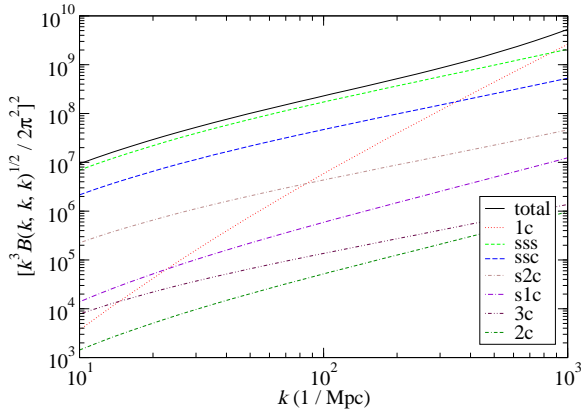


**Figure 9.** The one-halo term of the equilateral bispectrum separated into the contributions from each of the terms in equations (A10)–(A15). The order of the lines in the legend matches the order at \$k = 10^3 \text{ Mpc}^{-1}\$.

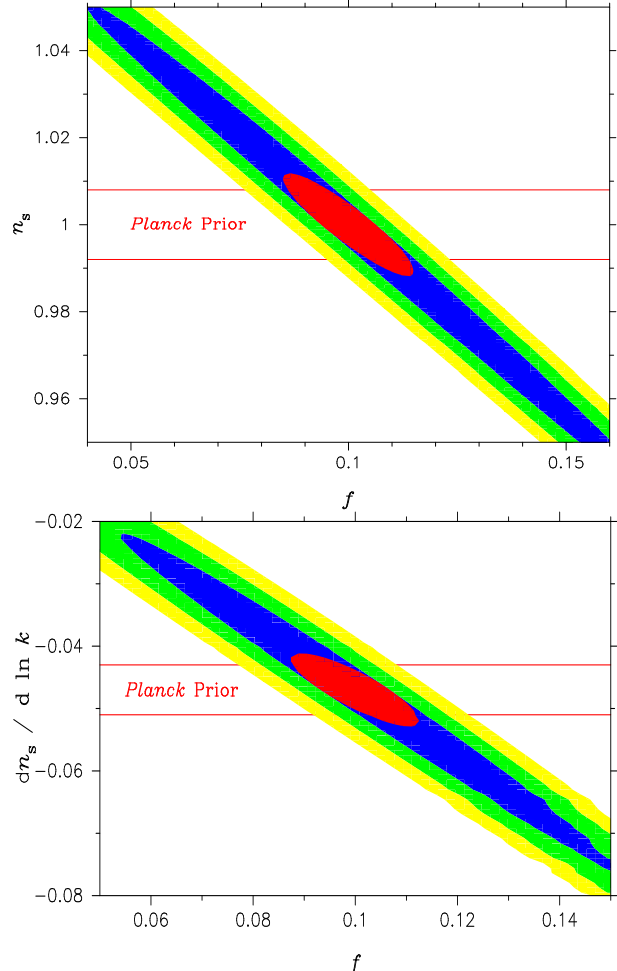


**Figure 10.** Contour plots on two-dimensional planes through \$\chi^2\$-space (no marginalization). In the upper panel, the spectral index and substructure mass fraction vary with no running spectral index; in the lower panel, the spectral index is fixed at \$n\_s = 0.93\$ and a running parameter is varied along with the substructure mass fraction. The innermost contour of each plot is a one-sigma contour where we have applied prior constraints as expected from the *Planck* mission: \$\sigma\_{n\_s} = 0.008\$ and \$\sigma\_{dn\_s/d \ln k} = 0.004\$ (Eisenstein et al. 1998). The other contours are one-, two- and three-sigma with no priors.

et al. (2003) quite well. Higher-resolution *N*-body simulations are needed to test our model.

We agree with Huffenberger & Seljak (2003) that a concentration parameter distribution alone cannot resolve the discrepancy between the halo model and Smith et al. (2003). We have shown, however, that the distribution increases power on small scales by about 10 per cent, which is comparable to the accuracy of the Smith et al. formula. Hence the scatter in the concentration parameter needs to be taken into account on scales smaller than \$k = 10 \text{ Mpc}^{-1}\$.

Our examination of the prospects for parameter constraints are by no means complete. A more careful treatment must marginalize over a larger parameter space \$\chi^2(\Omega\_m, \Omega\_b, \Omega\_\nu, \sigma\_8, n\_s, dn\_s/d \ln k, f, \dots)\$, and account for survey limitations such as intrinsic alignment of source galaxies, the limits imposed by galaxy deblending issues and B-mode contamination. Most parameters, like \$\Omega\_m\$ and \$\sigma\_8\$, are not very degenerate with substructure, since they affect the power spectrum and bispectrum on all scales, while substructure modifies the

statistics only on small scales. Such parameters can be well constrained from large scale information and probably not confuse a measurement of  $f$ . Moreover, other observations constrain  $\Omega_m$  and  $\sigma_8$ , such as the cosmic microwave background, supernovae observations, galaxy clusters and galaxy clustering statistics.

The situation is similar for neutrino mass and baryon fraction, though to a somewhat lesser extent. While these parameters affect the lensing power spectrum they also produce some suppression on scales with  $l < 10^4$  where substructure has little effect. This will help us to constrain  $\Omega_\nu$ ,  $\Omega_b$  and  $f$  separately. The *WMAP* results suggest that neutrinos are less massive than 0.2 eV (Spergel et al. 2003). We have shown that the power spectrum is much less sensitive to such neutrinos than substructure at the 10 per cent level (Fig. 6). With regard to baryons, their abundance is well constrained from CMB data and big-bang nucleosynthesis. Future observations are expected to reveal baryon oscillations in the weak-lensing signal which will allow for even tighter constraints on the baryon abundance.

The effects of the parameters  $c_0$ ,  $\beta$  and  $\alpha$ , which denote the normalization and slope of the halo concentration and the inner slope of the halo profile, can be separated from substructure effects with information from the reduced bispectrum. As we noted in Sec. 3, substructure produces a proportionately larger increase in the power spectrum than in the equilateral bispectrum. The result is that substructure amplifies the power spectrum, but attenuates the reduced bispectrum. This differs from the behavior of  $c_0$ ,  $\alpha$  and  $\beta$ , as demonstrated by Takada & Jain (2003), who find that these two parameters change the power spectrum and reduced bispectrum in the same sense.

Of the parameters considered, the tilt and run of the primordial power spectrum appear to produce an effect most similar to halo substructure. Our analysis in the previous section shows that the next generation of weak-lensing surveys will likely provide interesting  $n_s - f$  and  $dn_s/d\ln k - f$  constraints. Applying priors such as results from the *Planck* mission to these constraints should allow a detection of substructure. We find that a substructure mass fraction constraint at the  $\pm 2$  per cent is possible if observational errors can be controlled.

Numerical simulations indicate that, as a result of tidal disruptions in particular, a modified NFW profile for the distribution of subhaloes in the parent halo may be more appropriate. As we have already pointed out, simulations have not yet provided us with a definitive substructure-abundance profile for the centre-most regions of halos. Even taking the abundance to be zero within a core radius of order 10 kpc, as in Chen et al. (2003), we would redistribute only 4 per cent of our subhaloes. So while the magnitude of the  $P_{sc}$  term may be decreased by this order on 100-Mpc $^{-1}$  scales, smaller scales are dominated by the  $P_{1c}$  contribution (cf. Fig. 2), which does not depend on the subhalo distribution.

We thank Gary Bernstein and Ravi Sheth for helpful discussions. This work is supported in part by NASA through grant NAG5-10924 and NSF through grant AST03-07297.

## REFERENCES

Bardeen J. M., Bond J. R., Kaiser N., Szalay A. S., 1986, ApJ, 304, 15

Bartelmann M., Schneider P., 2001, Phys. Rep., 340, 291

Bullock J. S., Kolatt T. S., Sigad Y., Somerville R. S., Kravtsov A. V., Klypin A. A., Primack J. R., Dekel A., 2001, MNRAS, 321, 559

Chen J., Kravtsov A. V., Keeton C. R., 2003, ApJ, 592, 24

Cooray H., Hu W., 2001, ApJ, 554, 56

Cooray A., Sheth R., 2002, Phys. Rep., 372, 1

Eisenstein D. J., Hu W., Tegmark M., 1998, ApJ, 518, 2

Ghigna S., Moore B., Governato F., Lake G., Quinn T., Stadel J., 2000, ApJ, 544, 616

Henry J. P., 2000, ApJ, 534, 565

Hu W., Kravtsov A. V., 2003, ApJ, 584, 702

Huffenberger K. M., Seljak U., 2003, MNRAS, 340, 1199

Jing Y. P., 2000, ApJ, 535, 30

Kaiser N., 1992, ApJ, 388, 272

Klypin A., Kravtsov A. V., Valenzuela O., Prada F., 1999, ApJ, 522, 82

Kochanek C. S., Dalal N., 2003, ApJ, submitted (astro-ph/0302036)

Limber D. N., 1953, ApJ, 117, 134

Ma C. P., Fry J. N., 2000, ApJ, 543, 503

Mao S., Schneider P., 1998, MNRAS, 295, 587

Massey R., et al., 2004, preprint (astro-ph/0304418)

Meiksin A., White M., 1999, MNRAS, 308, 1179

Moore B., Ghigna S., Governato F., Lake G., Quinn T., Stadel J., Tozzi P., 1999a, ApJ, 524, L19

Moore B., Quinn T., Governato F., Stadel J., Lake G., 1999b, MNRAS, 310, 1147

Navarro J., Frenk C., White S. D. M., 1997, ApJ, 490, 493

Neyman J., Scott E. L., 1952, ApJ, 116, 144

Peacock J. A., Smith R. E., 2000, MNRAS, 318, 1144

Scherrer R. J., Bertschinger E., 1991, ApJ, 187, 425

Scoccimarro R., Sheth R., Hui L., Jain B., 2001, ApJ, 546, 20

Seljak U., 2000, MNRAS, 318, 203

Sheth R. K., Jain B., 2003, MNRAS, 345, 529

Sheth R. K., Tormen G., 1999, MNRAS, 308, 119

Smith R. E. et al., 2003, MNRAS, 341, 1311

Spergel D. N. et al., 2003, ApJS, 148, 175

Sugiyama N., 1995, ApJS, 100, 281

Takada M., Jain B., 2003, MNRAS, 340, 580

Tormen G., Diaferio A., Syer D., 1998, MNRAS, 299, 728

White M., 2002, ApJS, 143, 241

Zehavi I. et al., 2004, ApJ, 608, 16

## APPENDIX A: HALO-MODEL EXPRESSIONS WITH SUBSTRUCTURE

We present here the full expressions for the halo-model power spectrum and bispectrum. These expressions are derived in detail in Sheth & Jain (2003).

In the halo-model formalism, the power spectrum is expressed as a sum of one- and two-halo terms:

$$P(k) = P_{1h}(k) + P_{2h}(k). \quad (\text{A1})$$

We add substructure by expressing the one-halo term as

$$P_{1h} = P_{ss} + P_{sc} + P_{1c} + P_{2c}, \quad (\text{A2})$$

where

$$P_{ss}(k) = \int dM \frac{dN(M)}{dM} \left( \frac{M_s}{\bar{\rho}} \right)^2 U^2(k; M_s) \quad (\text{A3})$$

represents correlations between the smooth component of a halo. This term looks like the one-halo term of a halo model without substructure, but note that the mass of this smooth component is smaller by a fraction  $f$ , since  $M_s = (1 - f)M$ . Hence,  $P_{ss}$  is, for all  $k$ , less than the one-halo term calculated ignoring substructure. It is up to the remaining substructure terms in equation (A2) to make up for this loss.

$$P_{sc}(k) = 2 \int dM \frac{dN(M)}{dM} \frac{M_s}{\bar{\rho}} U(k; M_s) U_c(k; M_s) \int dm \frac{dn(m; M)}{dm} \frac{m}{\bar{\rho}} u(k; m) \quad (\text{A4})$$

denotes correlations between the smooth component and a subclump. The factor of 2 arises because either of the two density elements of the two-point function may lie in a subclump.

$$P_{1c}(k) = \int dM \frac{dN(M)}{dM} \int dm \frac{dn(m; M)}{dm} \left( \frac{m}{\bar{\rho}} \right)^2 u^2(k; m) \quad (\text{A5})$$

represents correlations where both elements lie in the same subclump and

$$P_{2c}(k) = \int dM \frac{dN(M)}{dM} U_c^2(k; M_s) \left[ \int dm \frac{dn(m; M)}{dm} \frac{m}{\bar{\rho}} u(k; m) \right]^2 \quad (\text{A6})$$

describes correlations between different subclump. Though this expression assumes that subclumps obey a Poisson distribution, we do not consider it important since this contribution to the power spectrum is subdominant (see Fig. 2).

Finally,

$$P_{2h}(k) = \int dM_1 \frac{dN(M_1)}{dM_1} \frac{M_1}{\bar{\rho}} U(k; M_1) \int dM_2 \frac{dN(M_2)}{dM_2} \frac{M_2}{\bar{\rho}} U(k; M_2) P(k; M_1, M_2) \quad (\text{A7})$$

is the two-halo term. Note that we have ignored substructure for this contribution; on large scales we trust the approximation of smooth NFW haloes with no substructure.

The one-halo term of the bispectrum has a similar division:

$$B_{1h} = B_{sss} + B_{ssc} + B_{s1c} + B_{s2c} + B_{1c} + B_{2c} + B_{3c}. \quad (\text{A8})$$

$$B_{sss}(k_1, k_2, k_3) = \int dM \frac{dN(M)}{dM} \left( \frac{M_s}{\bar{\rho}} \right)^3 U(k_1; M_s) U(k_2; M_s) U(k_3; M_s) \quad (\text{A9})$$

is the contribution with all three density elements, i.e. all three vertices of the triangle, in the smooth component of a halo.

$$\begin{aligned} B_{ssc}(k_1, k_2, k_3) = & \int dM \frac{dN(M)}{dM} \left( \frac{M_s}{\bar{\rho}} \right)^2 U(k_1; M_s) U(k_2; M_s) U_c(k_3; M_s) \\ & \times \int dm \frac{dn(m; M)}{dm} \frac{m}{\bar{\rho}} u(k_3; m) \\ & + \text{cyclic } k_i \text{ permutations} \end{aligned} \quad (\text{A10})$$

places only one vertex of the triangle in a subclump.

$$\begin{aligned} B_{s1c}(k_1, k_2, k_3) = & \int dM \frac{dN(M)}{dM} \frac{M_s}{\bar{\rho}} U(k_1; M_s) U_c(k_1; M_s) \\ & \times \int dm \frac{dn(m; M)}{dm} \left( \frac{m}{\bar{\rho}} \right)^2 u(k_2; m) u(k_3; m) \\ & + \text{cyclic } k_i \text{ permutations} \end{aligned} \quad (\text{A11})$$

has one vertex in the smooth component and the other two in the same subclump.

$$\begin{aligned} B_{s2c}(k_1, k_2, k_3) = & \int dM \frac{dN(M)}{dM} \frac{M_s}{\bar{\rho}} U(k_1; M_s) \\ & \times \prod_{i=2}^3 U_c(k_i; M_s) \int dm_i \frac{dn(m_i; M)}{dm} \frac{m_i}{\bar{\rho}} u(k_i; m_i) \\ & + \text{cyclic } k_i \text{ permutations} \end{aligned} \quad (\text{A12})$$

has one vertex in the smooth component and the other two in different subclumps.

$$B_{1c}(k_1, k_2, k_3) = \int dM \frac{dN(M)}{dM} \int dm \frac{dn(m; M)}{dm} \left( \frac{m}{\bar{\rho}} \right)^3 u(k_1; m) u(k_2; m) u(k_3; m) \quad (\text{A13})$$

places all three vertices in the same subclump.

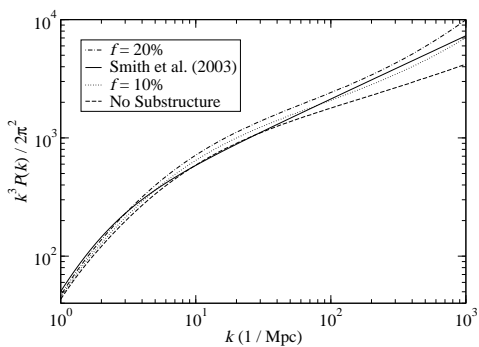
$$\begin{aligned} B_{2c}(k_1, k_2, k_3) = & \int dM \frac{dN(M)}{dM} U_c^2(k_1; M_s) \int dm_1 \frac{dn(m_1; M)}{dm_1} \frac{m_1}{\bar{\rho}} u(k_1; m_1) \\ & \times \int dm_2 \frac{dn(m_2; M)}{dm_2} \left( \frac{m_2}{\bar{\rho}} \right)^2 u(k_2; m_2) u(k_3; m_3) \\ & + \text{cyclic } k_i \text{ permutations} \end{aligned} \quad (\text{A14})$$

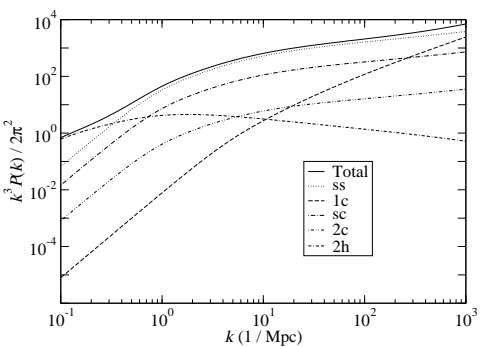
divides the three vertices between two subclumps.

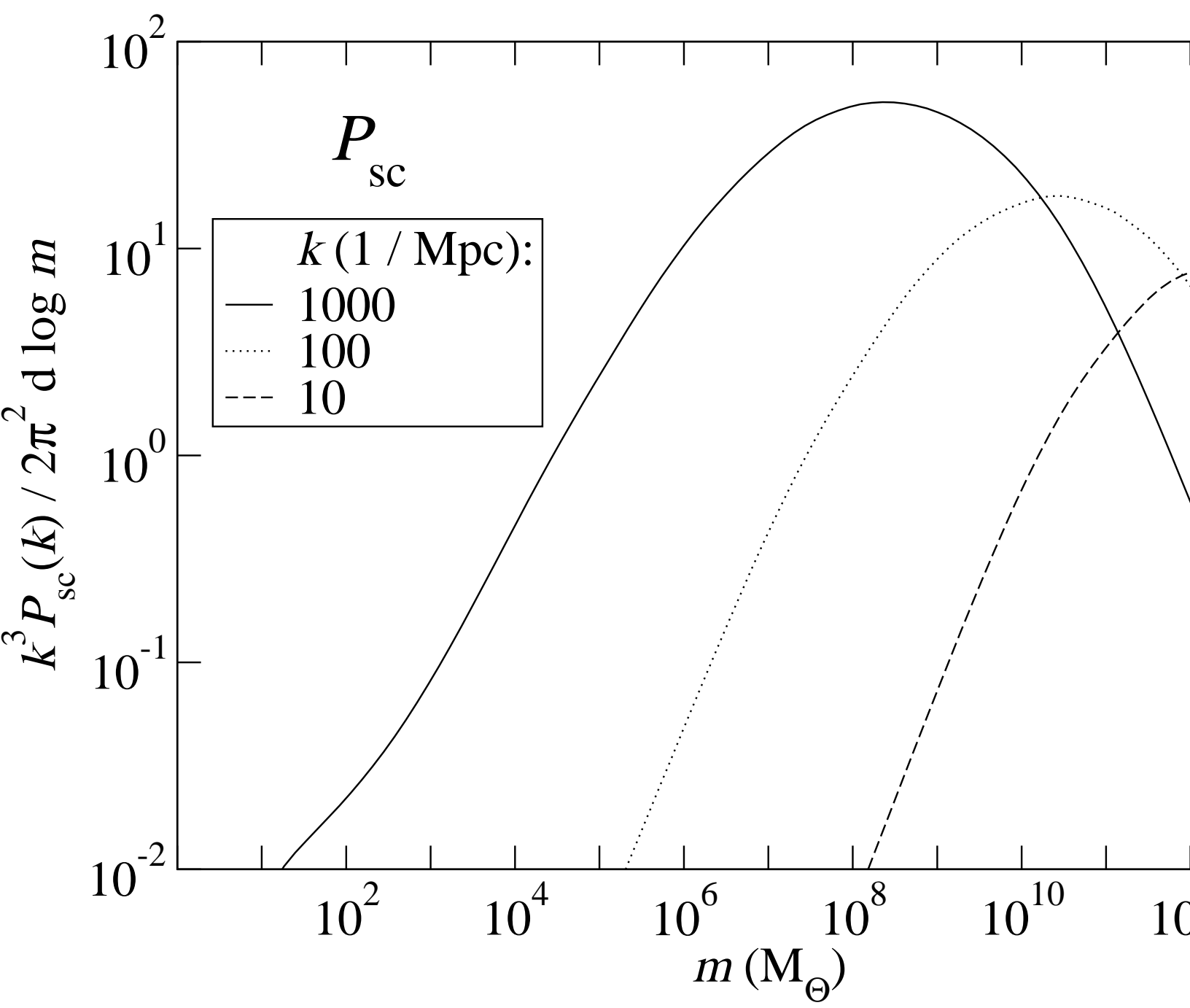
$$B_{3c}(k_1, k_2, k_3) = \int dM \frac{dN(M)}{dM} \prod_{i=1}^3 U_c(k_i; M_s) \int dm_i \frac{dn(m_i; M)}{dm_i} \frac{m_i}{\bar{\rho}} u(k_i; m_i) \quad (\text{A15})$$

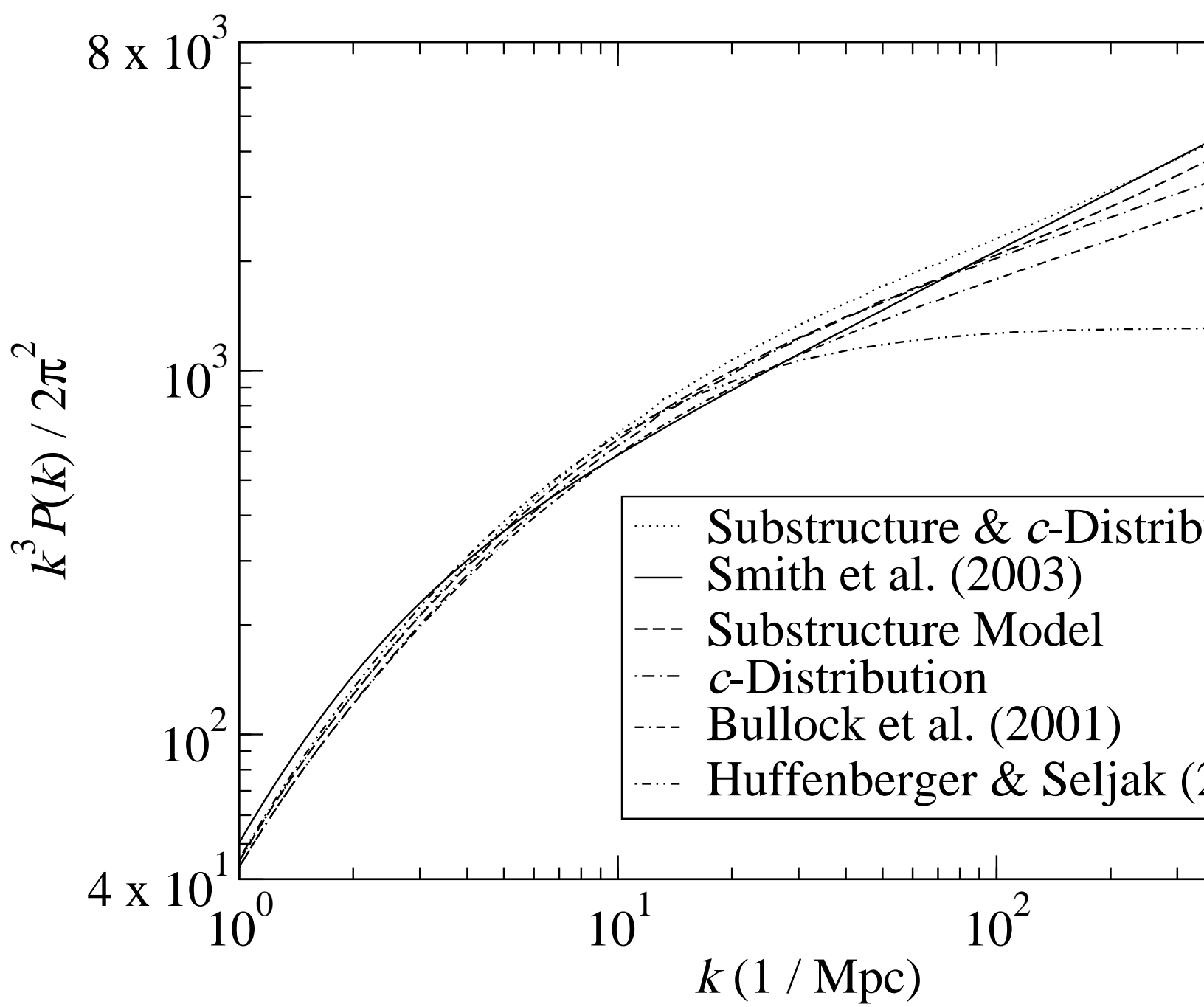
places the three vertices in different subclumps.

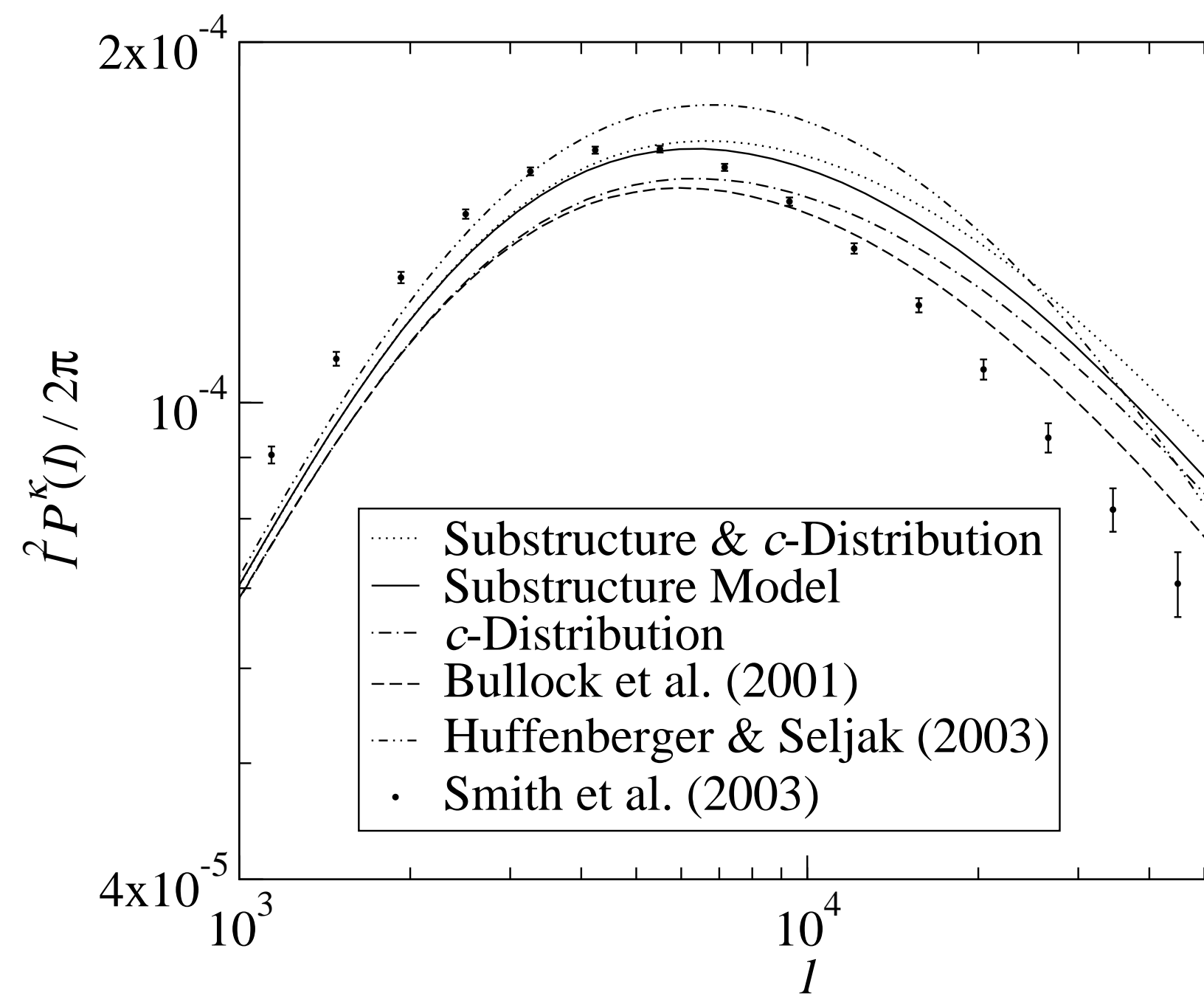
This paper has been typeset from a  $\text{\TeX}$ /  $\text{\LaTeX}$  file prepared by the author.

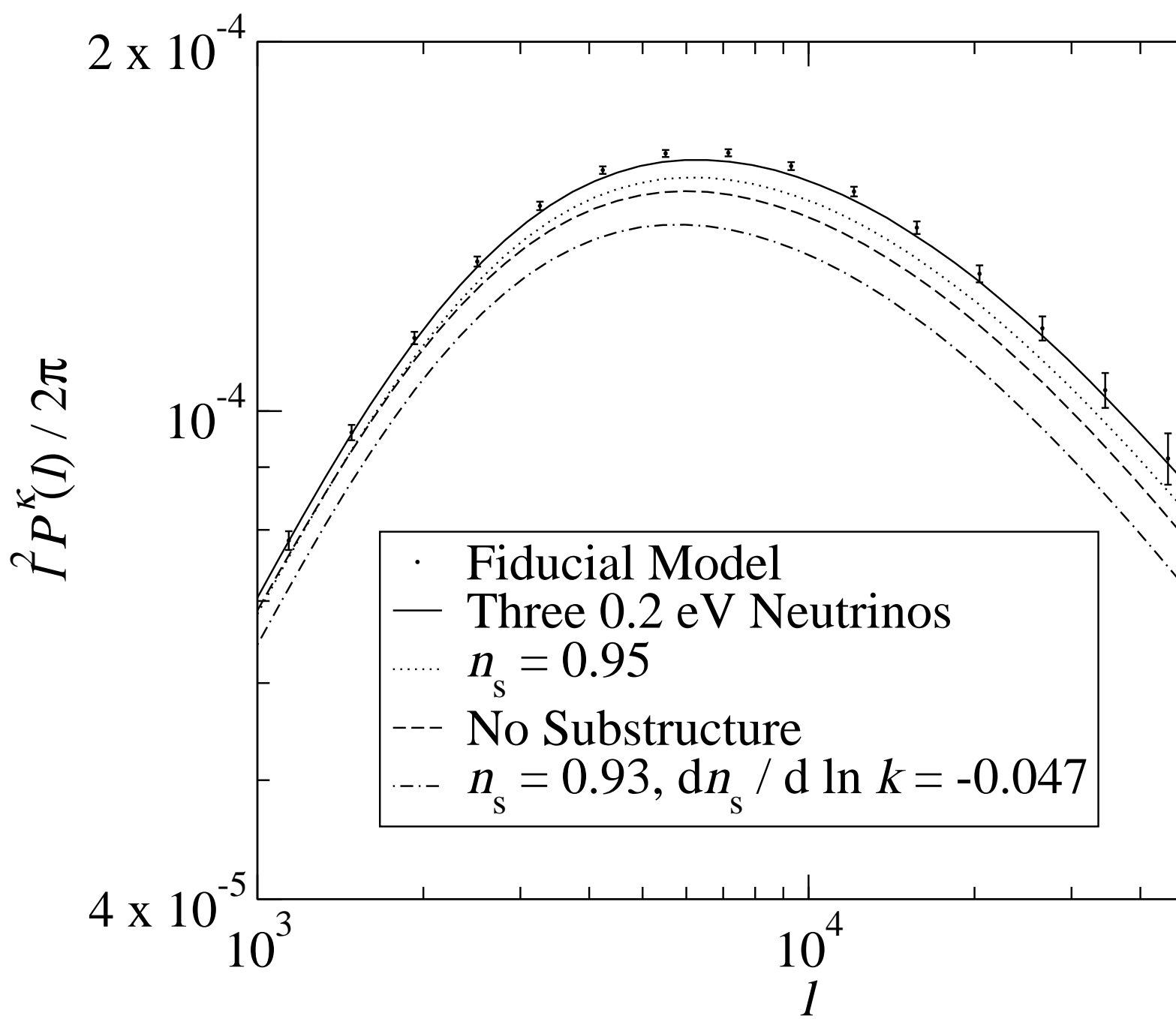


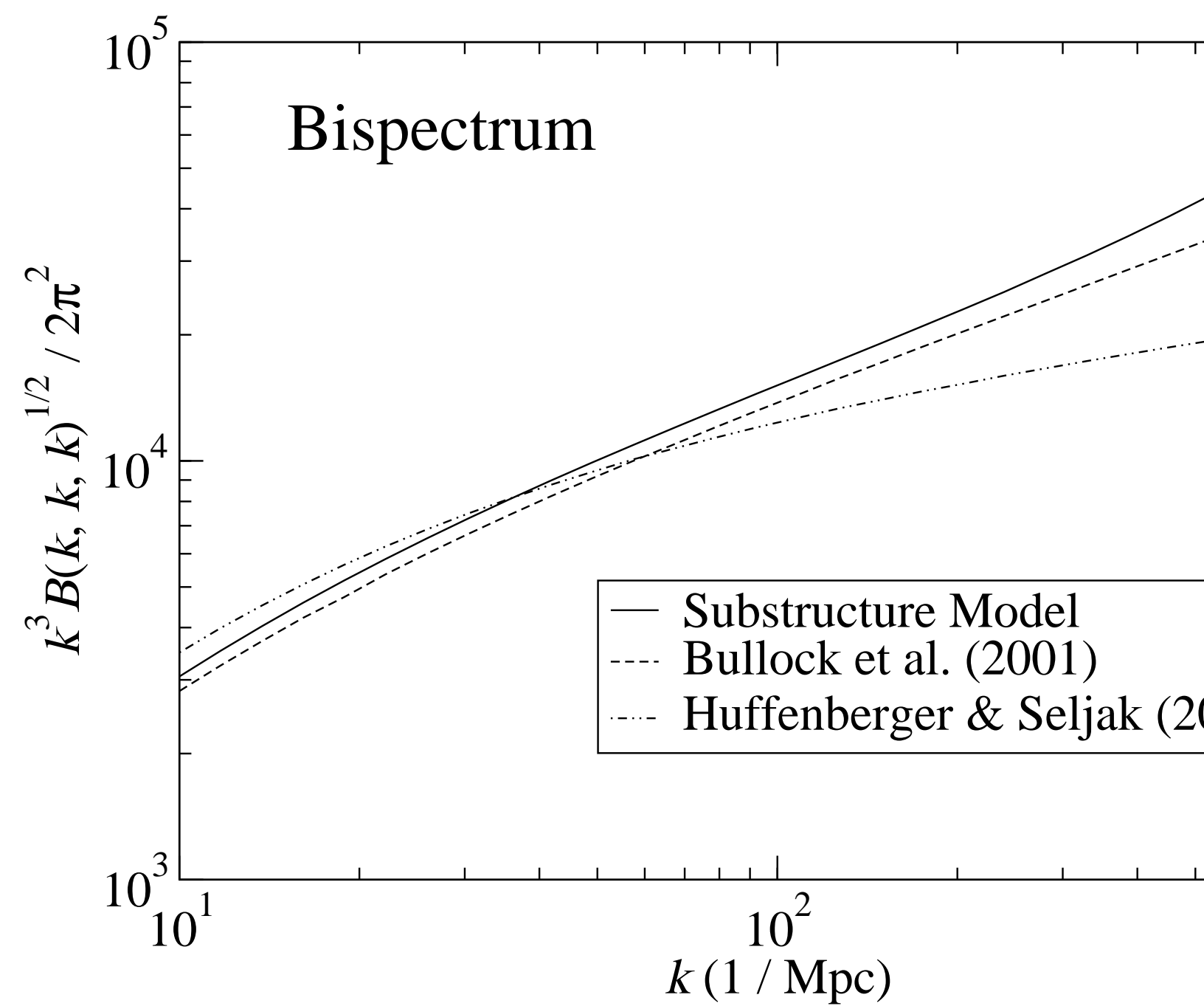


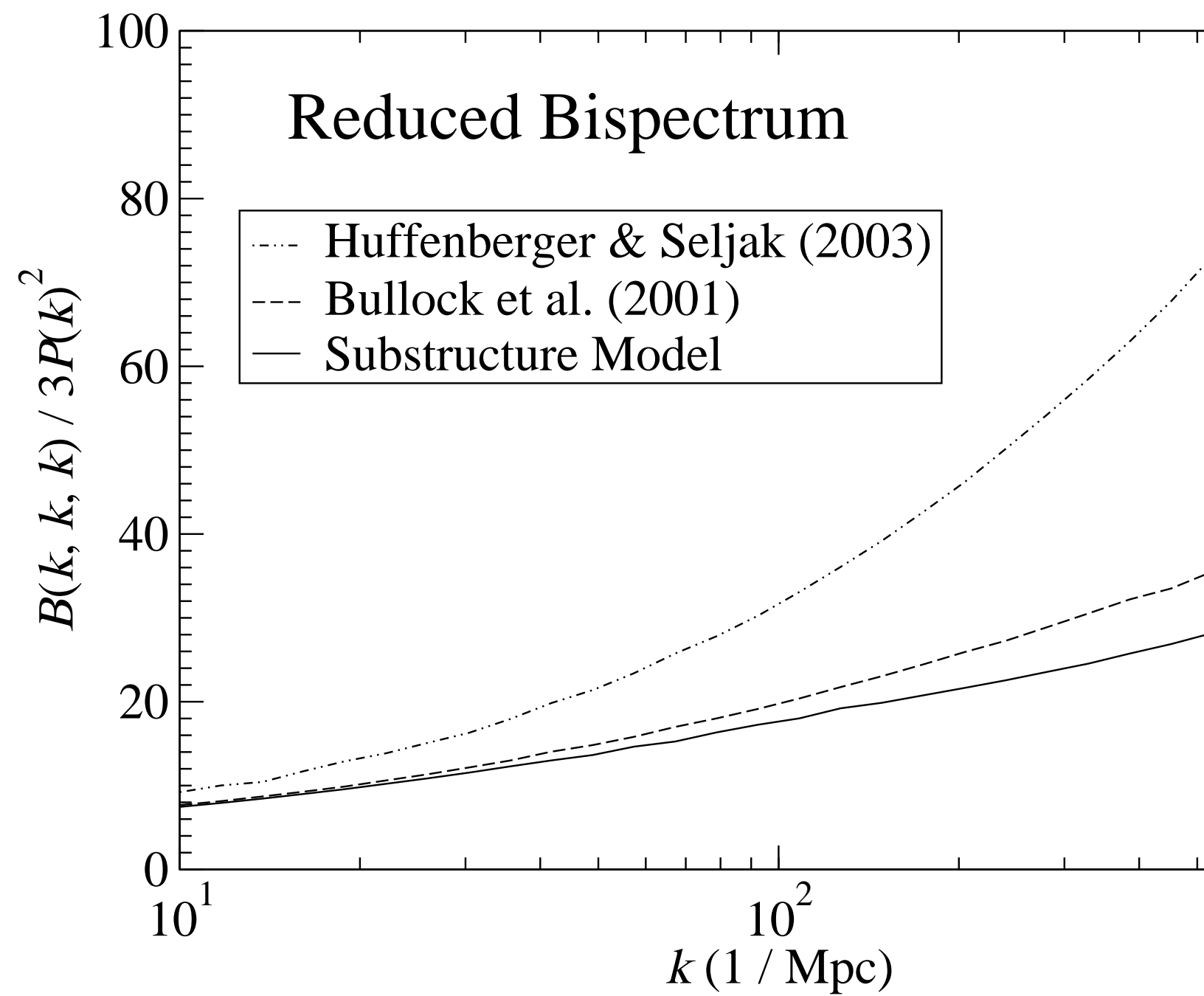


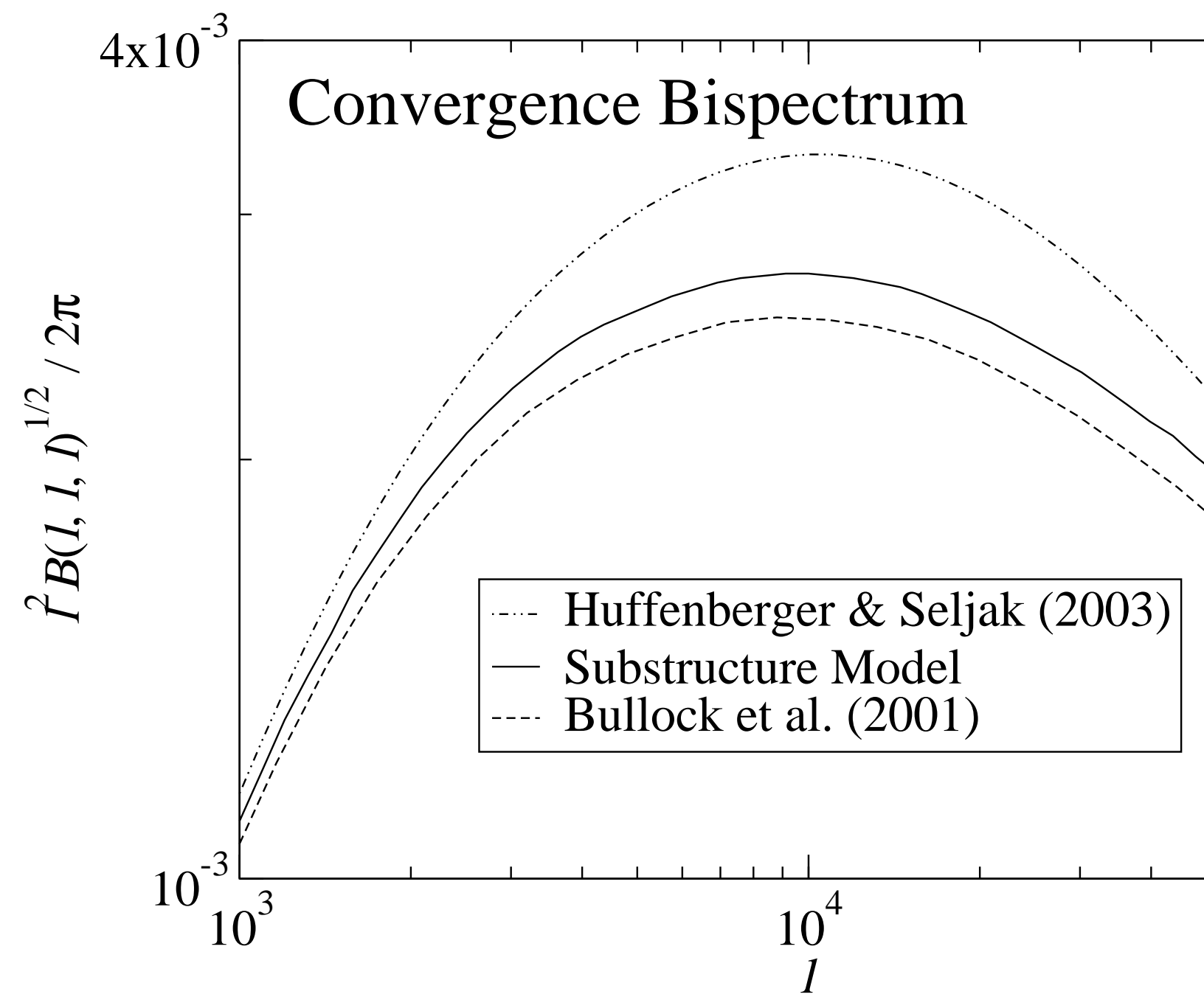












# Reduced Convergence Bispectrum

